Vibration Compensation and Precision Tracking of a Rotating Shaft by Nonlinear State Feedback*

Thomas R. Grochmal and Alan F. Lynch
Dept. of Electrical & Computer Engineering
University of Alberta
Edmonton, AB T6G 2V4, Canada
grochmal@ece.ualberta.ca, alanl@ieee.org

***Abstract*— In this paper, a nonlinear observer-based state feedback is derived to achieve precision tracking of a rotating shaft supported by active magnetic bearings (AMBs). Velocity and disturbance observers are constructed which operate in a hierarchical manner. This approach reduces the order of the design and modularizes compensation for synchronous vibration. Experimental results on a commercially available five degree-of-freedom system demonstrate accurate position tracking over the bearing air gap.**

***Index Terms*— Nonlinear control, nonlinear observers, disturbance, vibration control.**

I. Introduction

Control of AMBs is often based on a variation of Proportional-Derivative or state feedback. Such control schemes are easy to implement and provide sufficient performance for many applications requiring setpoint regulation [1]. Advances in control technology have enabled more complex strategies which can accomplish precise positioning of high speed rotating shafts. This have been motivated in part by industrial applications related to non-circular boring [2], [3], [4]. These applications require a sophisticated controller capable of vibration attenuation and trajectory tracking. The development of a control strategy that can satisfy these two objectives is the focus of this paper.

Vibration synchronous with the speed of rotation results primarily from mass unbalance, and is an obstacle to precise rotor positioning. Although mechanical balancing of the shaft can attenuate this effect, additional control action is required to further suppress it. Precision tracking control requires a synchronous position reduction method, which achieves forced rotation about the geometric axis by compensation of the harmonic unbalance forces. Existing solutions can often neglect AMB nonlinearity when the control objective is setpoint regulation and the coils are premagnetized. However, such designs based on linear approximate models may be too conservative when the objective is to track the shaft over a significant portion of the air gap [5]. To overcome this limitation, we design a nonlinear observer-based control treating synchronous vibration as a harmonic disturbance to be estimated. In this manner, we also compensate for model bias by estimation of a constant disturbance. Disturbance observers have been considered previously and incorporated into linear [6], sliding mode [7] and flatness-based [4] control designs. These proposed observers are usually high order (containing 5 to 10 states) and cannot decouple harmonic disturbance estimation and compensation from the rest of the controller. This decoupling is an asset for practical AMB systems because they operate in multiple stages (e.g. levitation, run-up, run-down) during which our modeling assumption of constant shaft speed may be invalid. As a result, cancelation of harmonic disturbances may be ineffective. Hence, to achieve low-order and modularity, we propose a hierarchical observer design. A reduced-order observer is constructed to estimate disturbances based on the availability of position and velocity. Velocity is estimated by an inner-loop observer with error dynamics that converge at a faster rate. We propose this design in the framework of a flatness-based tracking control.

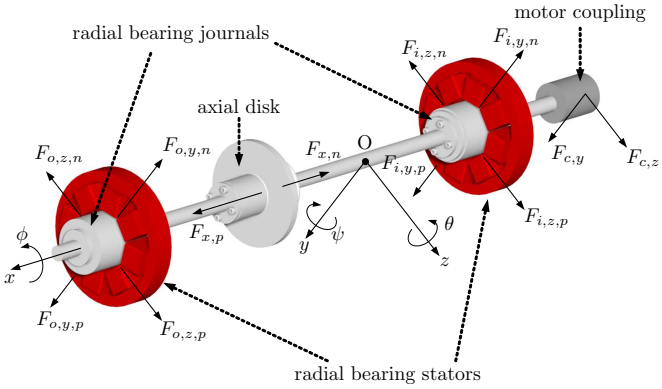

Fig. 1. Shaft assembly, motor coupling and radial bearing stators for a five DOF magnetic bearing system.

The AMB system under consideration was manufactured by *SKF Magnetic Bearings Inc.* (Calgary, AB) and is intended for testing control methodologies under no-load operation. The system offers several horizontal shaft configurations, and for the following work, a 305 mm $(12'')$ long, five DOF shaft assembly is chosen. Fig. 1 shows a CAD diagram of the shaft assembly with radial bearing stators. The assembly consists of a 9.5 mm $(3/8'')$ diameter shaft upon which are mounted two radial bearing rotors and an axial bearing disk. The assembly was determined to have

*This work is partially supported by the Natural Sciences and Engineering Research Council (NSERC) of Canada, Research Grant #249681-02.

negligible gyroscopic effects. The shaft is coupled to a DC motor by a flexible coupling. The system has a specified range of shaft speed of $2,000-10,000$ rpm. Some bearing specifications are provided in Table I.

Specification	radial bearing	axial bearing
static load cap.	76 N	205 N
saturation current	3.0 A	2.8 A
nominal gap	525 μm	783 μm
stator ID	35.1 mm	38.6 mm
stator OD	82.8 mm	71.4 mm
stator length	12.7 mm	13.5 mm
rotor OD	34.3 mm	66.0 mm

TABLE I

MAGNETIC BEARING SPECIFICATIONS

A modular dSPACE hardware system is used for control implementation. Inner-loop current control and outer-loop tracking control calculations are managed by the DSP board at a rate of 20 kHz. Three 16-bit ADC boards sample ten coil currents and rotor displacement along five axes. A digital output board generates PWM voltage waveforms for the drive circuitry. The coils are driven by custom-built power electronics. They consist of 10 H-bridges which deliver a maximum of 3 A output current per channel at 48 V. The switching frequency of the PWM amplifiers is 20 kHz.

III. Model Description

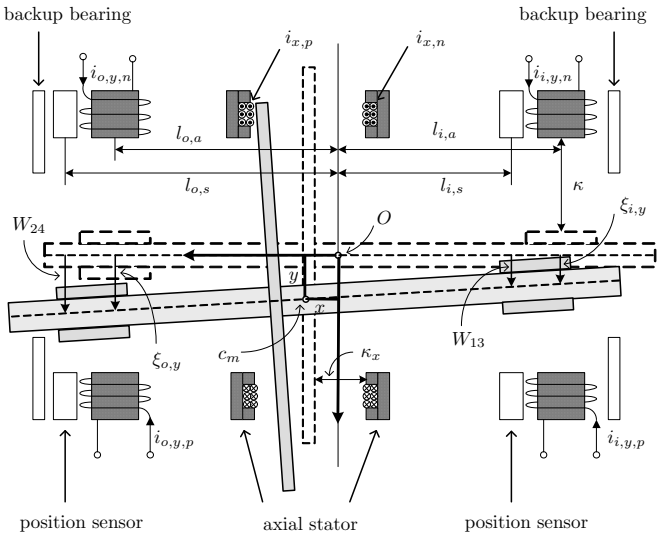

Fig. 2. Cross section of Figure 1 in the $x-y$ plane. Motor coupling not shown.

A standard nonlinear dynamic model is chosen as the basis for tracking control design. This model assumes a rigid shaft assembly. The dynamics equations are

$$m\ddot{x} = F_x \tag{1a}$$
$$m\ddot{y} = F_{o,y} + F_{i,y} + F_{c,y} + D_{c,y} + D_{h,y} \tag{1b}$$
$$m\ddot{z} = F_{o,z} + F_{i,z} + F_{c,z} + D_{c,z} + D_{h,z} \tag{1c}$$
$$J\ddot{\psi} = l_{i,a}F_{i,z} - l_{o,a}F_{o,z} + l_cF_{c,z} + \tau_{c,\psi} + \tau_{h,\psi} \tag{1d}$$
$$J\ddot{\theta} = l_{o,a}F_{o,y} - l_{i,a}F_{i,y} - l_cF_{c,y} + \tau_{c,\theta} + \tau_{h,\theta}. \tag{1e}$$

The variables x, y, z, ψ, θ represent the coordinates of the center of mass c_m of the shaft relative to an inertial frame with origin O. The parameters m and J denote the mass and transverse moment of inertia, respectively. Parameters $l_{o,a}, l_{i,a}$ are the distances from the outboard (subscript o) and inboard (subscript i) radial bearing stators to c_m, and it is assumed that $l_{o,a}, l_{i,a} \gg x$. Similarly, $l_{o,s}, l_{i,s}$ denote the distances from c_m to the outboard and inboard measurement planes. The distance l_c separates the motor coupling and c_m, and $F_{c,y/z}$[1] represent the linear spring forces resulting from deflection of the motor coupling. The spring force expressions are given by

$$F_{c,y} = -K(y - l_c\theta), \quad F_{c,z} = -K(z + l_c\psi). \tag{2}$$

The five magnetic bearing forces $F_x, F_{i/o,y/z}$ are each the sum of two forces from opposing coils which are denoted by their positive (subscript *p*) and negative (subscript *n*) components, see Fig. 1. The bearing force model is based on a horseshoe stator approximation and is given by the expression

$$\begin{aligned} F_{i/o,y/z} &= F_{i/o,y/z,p} - F_{i/o,y/z,n} \\ &= \frac{\beta i_{i/o,y/z,p}^2}{(\kappa - \xi_{i/o,y/z})^2} - \frac{\beta i_{i/o,y/z,n}^2}{(\kappa + \xi_{i/o,y/z})^2} \end{aligned} \tag{3}$$

for nominal air gap κ and force constant β. The control inputs are the coil currents denoted by $i_{i/o,y/z,p/n}$. The variables $\xi_{i/o,y/z}$ represent displacement of the radial rotors from the magnetic center. They are uniquely related to x, y, z, ψ, θ by the geometric relations

$$\begin{aligned} \xi_{o,y} &= y + l_{o,a}\theta + \sigma_{o,y}, & \xi_{o,z} &= z - l_{o,a}\psi + \sigma_{o,z} \\ \xi_{i,y} &= y - l_{i,a}\theta + \sigma_{i,y}, & \xi_{i,z} &= z + l_{i,a}\psi + \sigma_{i,z}. \end{aligned} \tag{4}$$

where $\sigma_{i/o,y/z}$ are magnetic offsets [13]. Mass unbalance enters the dynamics (1) as harmonic disturbance forces $D_{h,y/z}$ and torques $\tau_{h,\psi/\theta}$. Model bias and gravity are accounted for by constant disturbance forces $D_{c,y/z}$ and torques $\tau_{c,\psi/\theta}$. These disturbances are governed by the dynamics

$$\begin{aligned} \dot{D}_{c,y/z} &= 0, & \ddot{D}_{h,y/z} &= -\omega^2 D_{h,y/z} \\ \dot{\tau}_{c,\psi/\theta} &= 0, & \ddot{\tau}_{h,\psi/\theta} &= -\omega^2 \tau_{h,\psi/\theta}. \end{aligned} \tag{5}$$

where ω denotes constant shaft speed. The shaft speed and ten coil currents gives the system eleven inputs. The system's outputs are the rotor displacement along five axes: Z_{12} is the disk displacement along the x-axis, and $V_{13}, V_{24}, W_{13}, W_{24}$ represent the displacement of the radial rotors along the y- and z-axes in the planes of measurement $x = l_{o,s}$ and $x = -l_{i,s}$. The coordinates x, y, z, ψ, θ can be approximately recovered from the measurements $Z_{12}, V_{13}, V_{24}, W_{13}, W_{24}$ by the relations

$$\begin{aligned} \theta &= \frac{(W_{24} - W_{13})}{l_{o,s} + l_{i,s}}, \quad \psi = \frac{(V_{13} - V_{24})}{l_{o,s} + l_{i,s}} \\ x &= Z_{12}, \quad y = W_{13} + l_{i,s}\theta, \quad z = V_{24} + l_{o,s}\psi. \end{aligned} \tag{6}$$

Table II provides values for all model parameters.

[1]The term $F_{c,y/z}$ is compact notation that stands for $F_{c,y}, F_{c,z}$.

Param.	Value	Param.	Value
$l_{i,s}$	0.078 m	$l_{o,s}$	0.100 m
$l_{i,a}$	0.097 m	$l_{o,a}$	0.081 m
l_c	0.155 m	K	1200 N/m
J_x	$1.71 \cdot 10^{-4}$ kgm^2	J	$5.84 \cdot 10^{-3}$ kgm^2
β	$1.0 \cdot 10^{-6}$ Nm^2/A^2	β_x	$5.0 \cdot 10^{-6}$ Nm^2/A^2
κ	$5.25 \cdot 10^{-4}$ m	κ_x	$7.83 \cdot 10^{-4}$ m
m	0.98 kg		

TABLE II

MODEL PARAMETERS

IV. Flatness-Based Trajectory Tracking

The differential flatness [8] property of system (1) leads to a convenient design method for a nonlinear tracking controller [9], [10]. This flatness-based control is presented here in two steps. For the first step we design a control with bearing force as the input. In the second step we construct the control current based on the force control.

A. Force Control

For the $x-y$ plane subsystem (1b), (1e) we define a flat output (y, θ) and assume $F_{i/o,y}$ to be inputs. The feedback

$$F_{i/o,y} = \frac{m l_{o/i,a} \eta_y \mp J \eta_\theta - (l_{o/i,a} \pm l_c) F_{c,y}}{l_{o,a} + l_{i,a}} + F^{\text{dist}}_{i/o,y} \tag{7}$$

where $F^{\text{dist}}_{i/o,y}$ represents the disturbance compensating forces

$$F^{\text{dist}}_{i/o,y} = \frac{-l_{o/i,a}(D_{c,y} + D_{h,y}) \pm (\tau_{c,\theta} + \tau_{h,\theta})}{l_{i,a} + l_{o,a}}$$

gives the chains of integrators

$$\ddot{y} = \eta_y, \quad \ddot{\theta} = \eta_\theta$$

where η_y and η_θ represent auxiliary control variables. For the y coordinate, the auxiliary control

$$\eta_y = \ddot{y}_r - k_2(\dot{y} - \dot{y}_r) - k_1(y - y_r) \tag{8}$$

gives stable tracking error dynamics for controller gains $k_1, k_2 > 0$, where y_r is a reference trajectory at least twice differentiable with respect to time.

B. Current Control

Determining the control currents $i_{i/o,y,p/n}$ from the force feedback references (7) is equivalent to inverting the force relations (3). This inversion is non-unique for the following reasons:

1) the force-current relation in (3) is quadratic, and
2) the number of independently controlled coils (ten) exceeds the number of force components generated (five).

Solutions to this problem based on performance and power efficiency criteria have been extensively studied [11]. We adopt the widely applied constant current sum biasing scheme to maximize the force slew rate available to the bearing actuators [12]. Low- and zero-bias designs, which are common among nonlinear control schemes, have the potential to limit the dynamic response of the controller if voltage limits are not sufficiently high [13]. Hence the bearing force model (3), dropping subscripts, is re-expressed as

$$F = \frac{\beta(i_b + \Delta i)^2}{(\kappa - \xi)^2} - \frac{\beta(i_b - \Delta i)^2}{(\kappa + \xi)^2} \tag{9}$$

where i_b and Δi are the bias and differential currents respectively. Inversion of (9) yields [10]

$$\Delta i = \begin{cases} \frac{-\beta(\xi^2+\kappa^2) i_b - \beta(\xi^2-\kappa^2)\sqrt{F\xi\kappa/\beta + i_b^2}}{2\xi\beta\kappa} & \xi \neq 0 \\ F\kappa^2/(4\beta i_b) & \xi = 0. \end{cases} \tag{10}$$

The case for $\xi = 0$ is determined by applying l'Hôpital's Rule. To ensure a non-negative discriminant in (10), it is sufficient to impose the limits

$$-\frac{4\beta i_b^2}{(\kappa + \xi)^2} \leq F \leq \frac{4\beta i_b^2}{(\kappa - \xi)^2}$$

which are obtained by restricting $|\Delta i| \leq i_b$. Since each coil is limited by a saturation current I_s, peak force and maximum slew rate are obtained by setting $i_b = I_s/2$.

V. Hierarchical Observer Design

The control law (7) requires knowledge of position, velocity, and constant and harmonic disturbances. Since position is the only available measurement, we reconstruct estimates of velocity and disturbances by state observers. To jointly estimate velocity and disturbances would require a fifth order observer for each DOF. As an alternative approach, we propose a reduced-order disturbance observer based on the assumption that position and velocity are available. Then, we design an inner-loop velocity observer with error dynamics that is sufficiently faster than that of the disturbance observer.

A. Velocity Observer

We present the case for the y coordinate by a procedure that can be applied in a similar manner to each DOF. Ignoring constant and harmonic disturbances, we consider the simplified dynamics

$$m\ddot{y} = F_{o,y} + F_{i,y} + F_{c,y}$$

as the basis for an observer which estimates the time derivative of y. We define the acceleration $a_y(\Delta i_{i/o,y}, x, y, \theta) = (F_{o,y} + F_{i,y} + F_{c,y})/m$ which accounts for the spring coupling (2), and the nonlinearity of the bearing force relation (3), and is only a function of input and output. Estimates of displacement $\hat{y}$ and velocity $\hat{v}_y$ are obtained with the observer

$$\begin{pmatrix} \dot{\hat{y}} \\ \dot{\hat{v}}_y \end{pmatrix} = \begin{pmatrix} 0 & 1 \\ 0 & 0 \end{pmatrix} \begin{pmatrix} \hat{y} \\ \hat{v}_y \end{pmatrix} + \begin{pmatrix} 0 \\ 1 \end{pmatrix} a_y + \begin{pmatrix} \ell_1 \\ \ell_2 \end{pmatrix} (y - \hat{y}) \tag{11}$$

for observer gains $\ell_1, \ell_2 > 0$. Next, we show a sufficiently accurate estimate in the presence of bounded disturbances

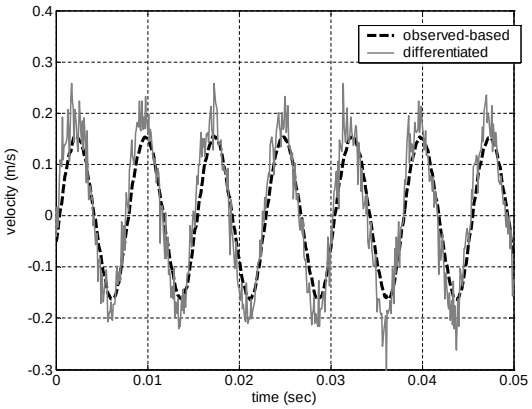

Fig. 3. Comparison of observer-based to numerically differentiated estimates of $\dot{y}$.

can be obtained. We define the estimation error vector $\zeta = (y - \hat{y}, \dot{y} - \hat{v}_y)^T$ and have error dynamics

$$\dot{\zeta} = \underbrace{\begin{pmatrix} -\ell_1 & 1 \\ -\ell_2 & 0 \end{pmatrix}}_{\bar{A}} \zeta + \underbrace{\begin{pmatrix} 0 \\ \frac{1}{m} \end{pmatrix}}_{\bar{B}} D_y \tag{12}$$

where $D_y = D_{c,y} + D_{h,y}$ and we have assumed the bound $|D_y| \leqslant \bar{D}$. From the solution of (12) we have

$$\begin{aligned} \zeta(t) &= V^{-1}(\lambda) e^{\Lambda t} V(\lambda) \zeta(0) \\ &\quad + \int_0^t V^{-1}(\lambda) e^{\Lambda(t-\tau)} V(\lambda) \bar{B} D_y(\tau) d\tau. \end{aligned} \tag{13}$$

where $\Lambda = \text{diag}[\lambda_1, \lambda_2] = V\bar{A}V^{-1}, \lambda_2 < \lambda_1 < 0$ and $V(\lambda)$ is a Vandemonde matrix. Taking the norm and computing an upper bound gives

$$\|\zeta(t)\| \leqslant \|V^{-1}(\lambda)\| \left[e^{\lambda_1 t} \|V(\lambda)\zeta(0)\| + \frac{\sqrt{2}\bar{D}}{m|\lambda_1|}(1 - e^{\lambda_1 t}) \right]$$

We take the limit to obtain a bound on the asymptotic error

$$\lim_{t \to \infty} \|\zeta(t)\| \leqslant \frac{\sqrt{2}\bar{D}}{m|\lambda_1|} \|V^{-1}(\lambda)\|. \tag{14}$$

There exists λ_1, λ_2 such that (14) can made arbitrarily small. For example, $\lambda_1 = -w, \lambda_2 = -w^2, w > 0$ results in $\lim_{w \to \infty} \|V^{-1}(-w, -w^2)\| / |-w| = 0$. To demonstrate the effectiveness of the observer (11), Fig. 3 compares the observed velocity $\hat{v}_y$ to a numerical differentiation of y at a rotational speed of $8,000$ rpm. The eigenvalues for the observer are -3500 and -4500. It is shown that the observer readily filters out high frequency noise.

B. Disturbance Observer

A reduced-order observer is constructed to obtain constant and harmonic disturbance estimates based on knowledge of position, velocity, and current, and without simplification of the dynamic equations. For the y subsystem, the observer is

$$\begin{aligned} \begin{pmatrix} \dot{z}_1 \\ \dot{z}_2 \\ \dot{z}_3 \end{pmatrix} &= \begin{pmatrix} -h_1 & -h_1 & 0 \\ -h_2 & -h_2 & 1 \\ -h_3 & -(h_3 + \omega^2) & 0 \end{pmatrix} \begin{pmatrix} z_1 \\ z_2 \\ z_3 \end{pmatrix} \\ &- \begin{pmatrix} h_1^2 + h_1 h_2 & h_1 \\ h_1 h_2 + h_2^2 - h_3 & h_2 \\ h_1 h_3 + h_2(h_3 + \omega^2) & h_3 \end{pmatrix} \begin{pmatrix} m\hat{v}_y \\ m a_y(\Delta i_{i/o,y}, x, y, \theta) \end{pmatrix} \\ \begin{pmatrix} \hat{D}_{c,y} \\ \hat{D}_{h,y} \end{pmatrix} &= \begin{pmatrix} z_1 \\ z_2 \end{pmatrix} + \begin{pmatrix} h_1 \\ h_2 \end{pmatrix} m\hat{v}_y \end{aligned} \tag{15}$$

where $h_i, 1 \leqslant i \leqslant 3$ are observer gains. Defining $D_{v,y} = \dot{D}_{h,y}$ and the estimation error vector as $(\tilde{D}_{c,y}, \tilde{D}_{h,y}, \tilde{D}_{v,y})^T = (D_{c,y} - \hat{D}_{c,y}, D_{h,y} - \hat{D}_{h,y}, D_{v,y} - \hat{D}_{v,y})^T$, we have the error dynamics

$$\begin{aligned} \begin{pmatrix} \dot{\tilde{D}}_{c,y} \\ \dot{\tilde{D}}_{h,y} \\ \dot{\tilde{D}}_{v,y} \end{pmatrix} &= \begin{pmatrix} -h_1 & -h_1 & 0 \\ -h_2 & -h_2 & 1 \\ -h_3 & -(h_3 + \omega^2) & 0 \end{pmatrix} \begin{pmatrix} \tilde{D}_{c,y} \\ \tilde{D}_{h,y} \\ \tilde{D}_{v,y} \end{pmatrix} \\ &\quad + \begin{pmatrix} h_1 \\ h_2 \\ h_3 \end{pmatrix} m\dot{\tilde{v}}_y. \end{aligned} \tag{16}$$

From (16) it is apparent that error in the velocity estimate $\tilde{v}_y$ enters the disturbance error system as a force $m\dot{\tilde{v}}_y$. To see the effect this has on disturbance estimates, we know from (12) that $\tilde{v}_y$, in steady state, is a signal with a constant and harmonic component so that $\tilde{v}_y(t) = \tilde{v}_{dc} + \tilde{v}_{ac} \sin(\omega t + \varphi)$. Hence $\dot{\tilde{v}}_y(t) = \omega \tilde{v}_{ac} \cos(\omega t + \varphi)$ in steady state. Next, consider the transfer matrix G with input $m\dot{\tilde{v}}_y$ and output $(\tilde{D}_{c,y}, \tilde{D}_{h,y})$. Calculating the magnitude of $G(s)$ at the synchronous frequency $s = j\omega$ gives $|G(j\omega)| = (0\ 1)^T$ which implies that $\lim_{t \to \infty} |\tilde{D}_{c,y}(t)| = 0$ and $\lim_{t \to \infty} |\tilde{D}_{h,y}(t)| \leqslant |m\omega\tilde{v}_{ac}|$. We can control the bound on $|\tilde{D}_{h,y}(t)|$ since $\tilde{v}_{ac}$ can be made arbitrarily small by the choice of eigenvalues for the velocity observer.

For a given ω and a desired characteristic polynomial $s^3 + \lambda_2 s^2 + \lambda_1 s + \lambda_0 = 0$ for the error dynamics (16), the observer gains are given by

$$h_1 = \frac{\lambda_0}{\omega^2}, \quad h_2 = \lambda_2 - \frac{\lambda_0}{\omega^2}, \quad h_3 = \lambda_1 - \omega^2.$$

Fig. 4 gives a block diagram of the closed loop system showing the cascade structure of the observers.

VI. Experimental Results

Experiments were performed to evaluate the performance of the proposed control scheme on a rotating shaft. It is important to note that shaft unbalance is significant for these experiments since the shaft is manually assembled and no balancing was performed, such as by mounting balance disks. Coils are biased at 1 A and eigenvalues of the tracking error dynamics are $-200 \pm 400i$. The eigenvalues of the disturbance observer are -55 and $-250 \pm 850i$ at the maximum shaft speed. Eigenvalues for the disturbance observer must be scheduled according to shaft speed to ensure a sufficiently high signal-to-noise ratio of the disturbance estimates.

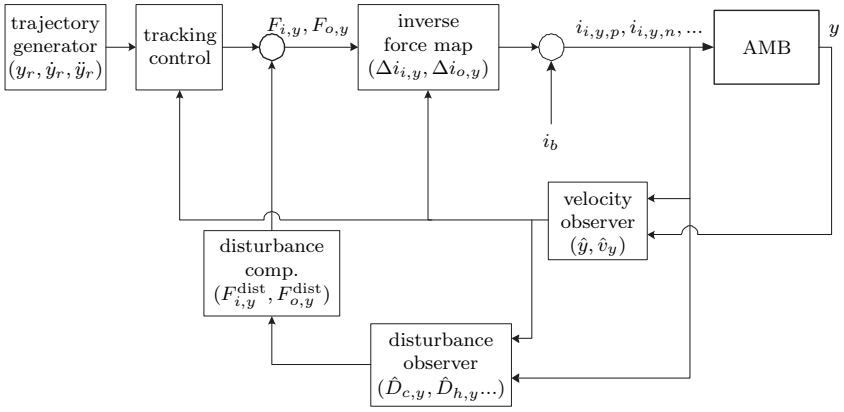

Fig. 4. Schematic of the closed loop system for the y coordinate.

A. Disturbance Rejection

For this experiment all reference trajectories were set to zero. Fig. 5 shows the outboard rotor orbital and coil currents during engagement of disturbance compensation at $10,000$ rpm. In steady state the rotor measurements $V_{13}, V_{24}, W_{13}, W_{24}$ are each constrained to an envelope of ± 1 μm centered about the origin. Fig. 5 shows spikes in the differential coil currents $\Delta i_{o,y/z}$ which indicate the high initial forces necessary to compensate for the harmonic disturbances. This figure shows that all available signal headroom has been used since the differential current peaks at the same magnitude as the bias current. Therefore, much greater unbalance forces cannot be tolerated by the control. After the transient, more efficient operation is apparent in the reduction of the synchronous component of the coil currents. Fig. 6 demonstrates the variation in harmonic disturbance attenuation according to shaft speed. A comparison of the vibration amplitude is made with and without disturbance compensation. We see from these results that in the worst case there is greater than 90% reduction in synchronous vibration and at best greater than 95% reduction. This additional control significantly improves the positioning of the shaft and increases the bearing clearances within which to track trajectories.

B. Trajectory Tracking

We demonstrate tracking with a trajectory that moves the center of mass c_m from the origin onto a 2.0 Hz elliptical orbit in a time $t = 1$ s:

$$\begin{aligned} y_r(t) &= 90 \cdot (r(t) - r(t-1)) \cdot \sin(4\pi t) \ \mu\text{m} \\ z_r(t) &= 40 \cdot (r(t) - r(t-1)) \cdot \cos(4\pi t) \ \mu\text{m} \\ x_r(t) &= \theta_r(t) = \psi_r(t) = 0 \ \mu\text{m}. \end{aligned} \tag{17}$$

where $r(t)$ is a unit ramp function. Tracking performance in the outboard measurement plane is shown in Fig. 7 at $10,000$ rpm. The orbital plot shows sufficiently good disturbance rejection to move the rotor over a large fraction of the available air gap (the system's nominal alarm setting for the radial bearings is 100 μm). Consistent tracking performance is also observed: the tracking error is less than about ± 2.5 μm. The tracking accuracy mainly depends on how well the shaft angular displacements ψ, θ can be stabilized. To this end, the main difficulty is compensation for the motor coupling which has a strong influence on the inboard radial bearing. The approximate linear spring model (2) was tuned online to achieve optimal performance. An AMB system with an inline motor would likely reduce tracking error.

VII. Conclusions

This paper has presented a nonlinear observer-based state feedback to track the motion of a rotating shaft. A hierarchical observer structure is proposed to simplify the overall design and to modularize compensation for synchronous vibration. Accurate positioning over the bearing air gap is demonstrated on a commercially available five DOF system.

Acknowledgment

The support of Carsten Collon (TU-Dresden, Germany) and Bill Bizuk (Bazooka Electronics, Edmonton, AB) is appreciated in constructing the test bench. The advice of Dr. Joachim Rudolph (TU-Dresden, Germany) is greatly appreciated.

References

[1] H. Bleuler, C. Gähler, R. Herzog, R. Larsonneur, T. Mizuno, R. Siegwart, and S.-J. Woo, "Application of digital signal processors for industrial magnetic bearings," *IEEE Trans. Contr. Syst. Technol.*, vol. 2, no. 4, pp. 280–289, Dec. 1994.

[2] B. Möller, "Using high-speed electrospindles with active magnetic bearings for boring of non-circular shapes," in *Proc.* 2^{nd} *ISMB*, Tokyo, Japan, 1990, pp. 189–196.

[3] M. Kim, T. Higuchi, T. Mizuno, and H. Hara, "Application of a magnetic bearing spindle to non-circular fine boring," in *Proc.* 6^{th} *ISMB*, Cambridge, MA, Aug. 1998, pp. 22–31.

[4] J. v. Löwis, J. Rudolph, J. Thiele, and F. Urban, "Flatness-based trajectory tracking control of a rotating shaft," in *Proc.* 7^{th} *ISMB*, ETH Zurich, Switzerland, Aug. 2000, pp. 299–304.

[5] N. Skricka and R. Markert, "Improvements in the integration of active magnetic bearings," *Contr. Eng. Pract.*, vol. 10, pp. 917–922, 2002.

[6] T. Higuchi, T. Mizuno, and M. Tsukamoto, "Digital control system for magnetic bearings with automatic balancing," in *Proc.* 2^{nd} *ISMB*, Tokyo, Japan, Jul. 1990, pp. 27–32.

[7] A. E. Rundell, S. V. Drakunov, and R. A. DeCarlo, "A sliding mode observer and controller for stabilization of rotational motion of a vertical shaft magnetic bearing," *IEEE Trans. Contr. Syst. Technol.*, vol. 4, no. 5, pp. 598–608, Sep. 1996.

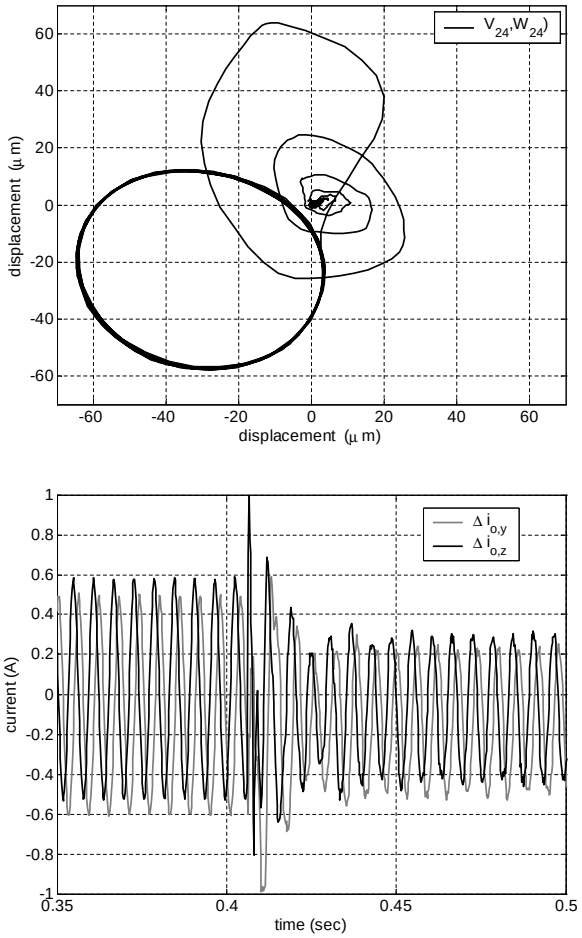

Fig. 5. Engagement of constant and harmonic disturbance compensation at a shaft speed of $10,000$ rpm.

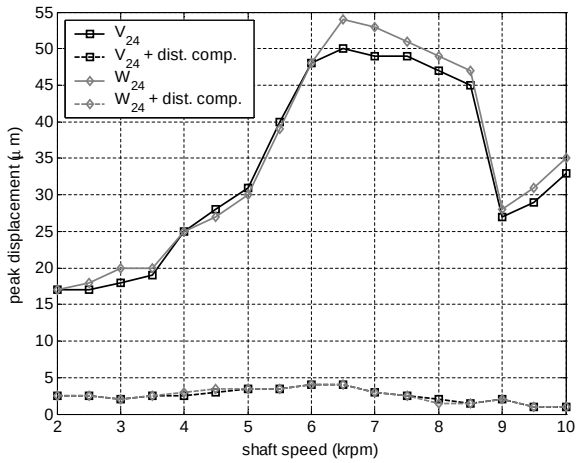

Fig. 6. Comparison of rotor vibration amplitude with and without disturbance compensation over the operating range of shaft speed.

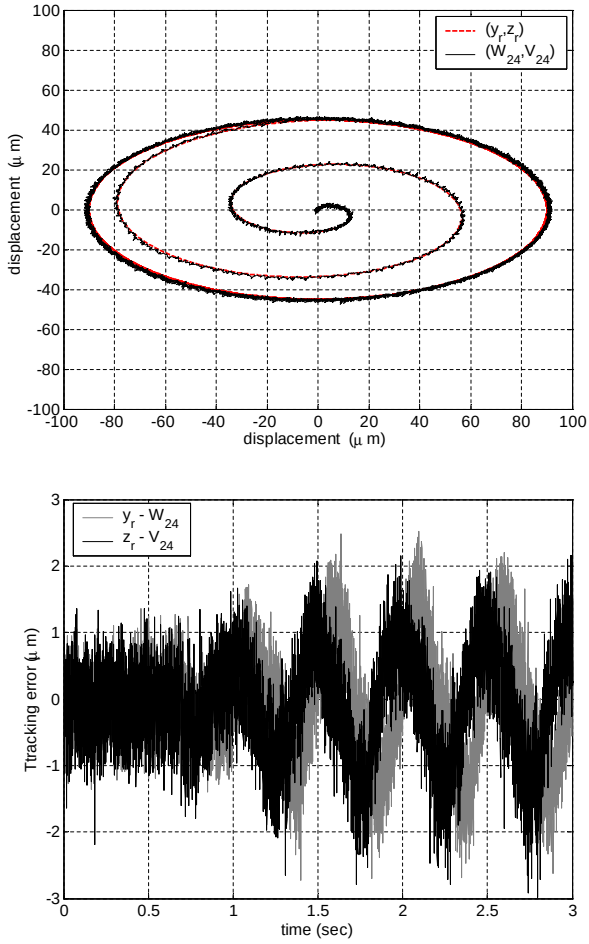

Fig. 7. Tracking performance at $10,000$ rpm.

[8] M. Fliess, J. Lévine, P. Martin, and P. Rouchon, "Flatness and defect of nonlinear systems: introductory theory and applications," *Int. J. Control*, vol. 61, no. 6, pp. 1327–1361, Jun. 1995.

[9] J. Lévine, J. Lottin, and J.-C. Ponsart, "A nonlinear approach to the control of magnetic bearings," *IEEE Trans. Contr. Syst. Technol.*, vol. 4, no. 5, pp. 524–544, Sep. 1996.

[10] J. v. Löwis, "Flachheitsbasierte Trajektorienfolgeregelung elektromechanischer Systeme," Ph.D. dissertation, TU Dresden, Germany, 2001.

[11] D. C. Meeker, "Optimal solutions to the inverse problem in quadratic magnetic actuators," Ph.D. dissertation, University of Virginia, 1996.

[12] C. R. Knospe and E. H. Maslen, "Introduction to active magnetic bearings," in *Short Course: Introduction to Magnetic Bearings*, C. R. Knospe, D. L. Trumper, and L. S. Stephens, Eds. University of Kentucky: Proc. 9th ISMB, Aug. 2004.

[13] T. R. Grochmal and A. F. Lynch, "Experimental comparison of nonlinear tracking controllers for active magnetic bearings," *Contr. Eng. Pract.*, 2006, in press.